Publication II

Minna Toivola, Fredrik Ahlskog, and Peter Lund. 2006. Industrial sheet metals for nanocrystalline dye-sensitized solar cell structures. Solar Energy Materials & Solar Cells, volume 90, number 17, pages 2881-2893.

Available online at www.sciencedirect.com
ScienceDirect
Solar Energy Materials & Solar Cells
ELSEVIER
Solar Energy Materials & Solar Cells 90 (2006) 2881–2893
www.elsevier.com/locate/solmat

# Industrial sheet metals for nanocrystalline dye-sensitized solar cell structures

Minna Toivola*, Fredrik Ahlskog, Peter Lund

*Laboratory of Advanced Energy Systems, Department of Engineering Physics and Mathematics, Helsinki University of Technology, P.O. Box 4100, FIN-02015 TKK, Finland*

Received 15 March 2005; accepted 1 May 2006
Available online 10 July 2006

**Abstract**

Direct integration of dye-sensitized solar cells (DSSC) onto industrial sheet metals has been studied. The stability of the metals, including zinc-coated and plain carbon steel, stainless steel and copper in a standard iodine electrolyte was investigated with soaking and encapsulation tests. Stainless and carbon steel showed sufficient stability and were used as the cell counter-electrodes, yielding cells with energy conversion efficiencies of 3.6% and 3.1%, respectively. A DSSC built on flexible steel substrates is a promising approach especially from the viewpoint of large-scale, cost-effective industrial manufacturing of the cells.


*Keywords:* Dye-sensitized solar cell; Metal substrate; Counter-electrode

## 1. Introduction

A significant part of the cost of photovoltaic (PV) systems is due to the additional structures needed in the installation and support of the panels. Considerable savings could be achieved if the PV systems were directly integrated into, e.g., roofing or other building materials. In addition, solar-active metal materials could widen up the product variety of the metal industry and speed up the commercialization of the new technology.

While the present mainstream silicon PV technology is difficult to integrate into roll-to-roll-produced metal materials as such, the more recent alternative thin film

*Corresponding author. Tel.: +358 9 4513217; fax: +358 9 4513195.
*E-mail address:* minna.toivola@tkk.fi (M. Toivola).

0927-0248/$ - see front matter © 2006 Elsevier B.V. All rights reserved.
doi:10.1016/j.solmat.2006.05.002

and nanostructured dye-sensitized solar cells (DSSC) could offer better possibilities. DSSC have also the advantages of being cost-efficient, non-toxic and most of the materials needed are easily available. In addition to that, the cells can be produced mostly in room temperature, atmospheric pressure and otherwise regular conditions.

Unlike the conventional semiconductor solar cells, a DSSC is a photoelectrochemical device consisting of two electrodes deposited on conducting substrates and connected by a layer of redox electrolyte. Electrical current is generated on the nanoporous titanium dioxide ($TiO_2$) photoelectrode where the dye molecules anchored onto the surface of the $TiO_2$ nanoparticles absorb the incoming photons and inject the electrons produced in this photoexcitation into the $TiO_2$ layer. The function of the redox electrolyte is to reduce the oxidized dye molecules back to the ground state to enable continuous electron production, a process in which the reduced form of the redox couple gets oxidized itself. The electrons are collected from the $TiO_2$ and transferred to the counter-electrode, where they complete the operating cycle of the cell by reducing the oxidized redox species back to its original state through an external load [1,2].

The standard approach in manufacturing DSSC has been to build them on conducting glass substrates. While the highest reported energy conversion efficiencies of the cells have been obtained with these substrates, glass has disadvantages especially from the view of large-scale industrial manufacturing of the cells. Replacement of the glass with other substrates such as light-weight and flexible plastic foils or metals would offer also cost reductions as the glass substrates constitute 15–20% of the total price of the cell [3]. Flexibility of the substrates is also an important requirement in the upscaling of the cell technology from laboratory to high-throughput industrial roll-to-roll production, whereas better electrical conductivity of the metals lowers the series resistance of the cells and thus increases the overall efficiency especially when the cell area increases. Replacing even one substrate with a non-fragile material such as metal also improves the long-term stability of the cells by lowering the risk of electrolyte leakage and material contamination by possible fractures in the glass.

DSSC substrate materials other than glass have been studied over the last few years (e.g. [4–22]). Metal substrates, though, have received considerably less attention than plastics. Ma et al. [17] and Fang et al. [18] studied stainless steel and nickel foils' stability as well as several types of conducting plastics in iodine electrolyte containing ionic liquid 1,2-dimethyl-3-propylimidazolium iodide. A 5% energy conversion efficiency was achieved with DSSC consisting of platinized stainless steel or nickel counter-electrodes and photoelectrodes deposited on FTO (fluorine-doped $SnO_2$)-coated glass. Kang et al. [19] used stainless steel foils as the photoelectrode substrate and achieved 4% energy conversion efficiencies after depositing the $TiO_2$ film on both indium–tin oxide (ITO)- and $SiO_x$-sputtered stainless steel and using chemically platinized conducting plastic as the counter-electrode, the electrolyte containing ionic liquid 1-vinyl-3-methylimidazolium iodide. Steel- and titanium-foil-based DSSC have been investigated also by Meyer et al. [20] who report 0.8% efficiency on a Ti-foil-based cell. Improvement of the DSSC efficiency by using zinc or titanium foils as the photoelectrode substrate is also mentioned in one patent [23] and some reports exist about depositing a $TiO_2$ film on a Ti sheet [24] and electrosynthetizing $TiO_2$ deposits on stainless steel [25], whereas to our knowledge standard industrial zinc-coated carbon steels employed as roofing materials have not been studied as DSSC substrates.

The objective of this research was to find out if DSSC could be directly integrated onto roll-to-roll produced standard industrial sheet metals. Materials supplied by metal industry such as different hot-dip zinc-coated steel, carbon steel, stainless steel and copper were studied as active substrates of the DSSC, i.e., these substrates acted simultaneously also as the counter-electrode of the cell.

One of the main problems in integrating the cells directly onto metal substrates is the standard liquid electrolyte used in the cells. Iodine, which is a crucial part of the electrolyte in the form of iodide/triiodide redox couple, is known to be chemically aggressive and possibly corrosive towards many metals. This is why the stability of the materials in the iodine electrolyte was tested with soaking and encapsulation tests, and finally the most suitable materials were selected for complete DSSC. The performance of the cells was characterized with *IV* curve measurements in a solar simulator and the charge transfer resistance between the metal counter-electrode and the electrolyte with electrochemical impedance spectroscopy (EIS). Charge transfer resistance gives information about the efficiency of the redox reaction between the iodide and triiodide ions occurring on the electrode–electrolyte interface thus indicating the electrode material's ability to function as a catalyst for this reaction.

Protective coatings of spray-pyrolyzed thin films of $TiO_2$ and ITO ($In_2O_3$:Sn) were tried on some materials to prevent the electrolyte from getting into direct contact with the underlying metal. However, these coatings turned out to be too porous on microscale and thus unreliable as corrosion protection against the liquid electrolyte. The research was therefore targeted to only those materials which did withstand the electrolyte as such, i.e., stainless and carbon steel. This resulted in good energy conversion efficiencies ($>3\%$; cf. 4–5% for all-glass substrate cells used as a reference in this study), compact and sturdy structures, and quick manufacturing process.

## 2. Experimental

The studied metal materials are listed in Table 1. "Corrosion protection coating" refers to the standard corrosion protection method offered by the manufacturer, and "storage protection" to the finishing treatment given to the otherwise ready product to prevent so-called white rust formation and other damages that might occur to the metal surface during storage.

Before use, the metal sheets were cut into 2 cm × 2 cm or 2.5 cm × 2.5 cm pieces and washed with water and mild detergent. After this, the cleansing was completed in an ultrasonic bath for 3 min first in ethanol and then in acetone. Finally, the pieces were dried with pressurized air.

Since metal oxides are usually more resistive against corrosion than pure metals, thermal treatment was also tried for some of the zinc-coated steel samples. To oxidize the coating, the metal plates were kept in an oven in 600 °C for 2 h.

### 2.1. Soaking and encapsulation tests

The soaking tests were performed by immersing the 2 cm × 2 cm metal pieces in 8 ml of standard iodine electrolyte consisting of 0.5 M LiI (Fluka), 0.05 M $I_2$ (Prolabo/Merck) and 0.5 M 4-*tert*-butyl-pyridine (TBP; Fluka) in 3-methoxypropionitrile (MePRN; Alfa-Aesar). The test bottles were closed tightly and kept in different environmental conditions: at room

Table 1
Metal materials used in the research

| Metal sheet | Composition | Corrosion protection coating[a] | Minimum mass of the coating[b] ($g/m^2$) | Storage protection | Average coating thickness[c] (μm) | Overall thickness (mm) | Supplier |
|---|---|---|---|---|---|---|---|
| Carbon steel | Fe | Zn | 275 | – | 20 | 1.00 | Ruukki, Ltd. |
| Carbon steel | Fe | Zn | 275 | Chromation | 20 | 1.00 | Ruukki, Ltd. |
| Carbon steel | Fe | Zn–Al (95%–5%) | 255 | Polymer coating | 16 | 0.80 | Ruukki, Ltd. |
| Carbon steel | Fe | Zn–Al (95%–5%) | 255 | Chromation | 16 | 1.00 | Ruukki, Ltd. |
| Carbon steel | Fe | – | – | – | – | 1.00 | Ruukki, Ltd. |
| Stainless steel (type 304/1.4301) | Fe 73.93%<br>Cr 18%<br>Ni 8%<br>$C_{max}$ 0.07% | – | – | – | – | 1.25 | Outokumpu, Ltd. |
| Copper | Cu | – | – | – | – | 0.63 | Outokumpu, Ltd. |

[a]Application method: hot dipping.
[b]Calculated per 1 $m^2$ metal sheet, including both surfaces.
[c]Triple-spot test; variation ca. $\pm 5\,\mu m$.

temperature in direct sunlight, normal room light and in dark. In order to find out the dissolving rate of the metals into the electrolyte, the concentration of metal ions in it was analyzed with atomic absorption spectrometry (AAS) after 6 weeks and for some samples after 11 weeks of soaking.

Encapsulation tests were performed to mimic more closely the real situation in the cells. Test cells were built by sealing a 2.5 cm × 2.5 cm metal plate together with a glass piece of the same or slightly smaller size using thermoplastic polymer film (Surlyn®, DuPont) as a spacer. Electrolyte was inserted into the cells through thin filling channels cut into the Surlyn film after which the ends of the channels were sealed with vacuum sealant (TorrSeal®, Varian Vacuum Technologies). The seams between the metal and glass were also sealed with the vacuum sealant to make sure the cell was air-tight and no electrolyte could leak out. Fig. 1 presents a schematic of the test cell.

### 2.2. Complete solar cells

A schematic of the DSSC used in this study is presented in Fig. 2. Stainless and carbon steel plates were used as counter-electrodes both with and without platinization. Platinization was performed by dropping a few drops of 5 mM solution of $PtCl_4$ (Aldrich) in 2-propanol onto the plates with a pipette, after which the solvent was let to evaporate and the dry plates were fired in an oven in 385 °C for 10–15 min. Platinized FTO-coated glass (Pilkington TEC 15, sheet resistance 15 Ω/sq., supplied by Hartford Glass Company, Inc.) counter-electrodes were prepared with the same technique for a reference.

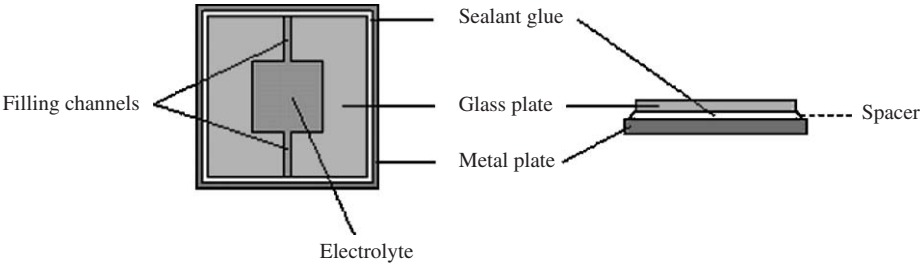


Fig. 1. Encapsulation of electrolyte on a metal plate.

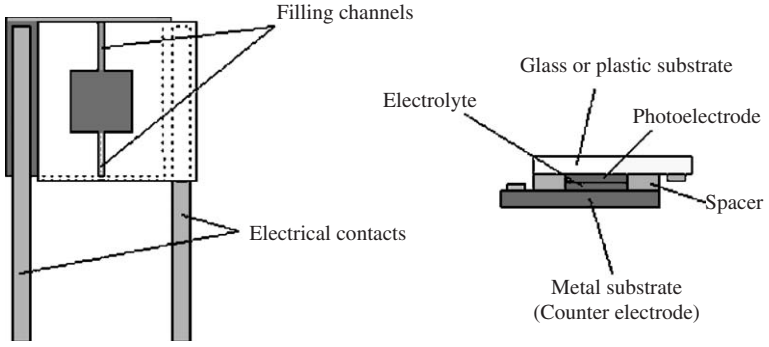


Fig. 2. The geometry of the dye-sensitized solar cell.

Photoelectrodes were prepared both on FTO glass and ITO-PET plastic substrates (NV-CT-CH-1S-M-7, sheet resistance 60 Ω/sq., supplied by Bekaert Specialty Films, Inc.). Glass photoelectrodes were prepared by spreading two layers of commercial $TiO_2$ paste (Sustainable Technologies International) on the glass substrates with the doctor-blading method using a 4 mm × 8 mm rectangular mask cut of regular office tape. Plastic photoelectrode films were prepared by spray deposition of 20 wt% ethanol solution of $TiO_2$ nanoparticles (P25, Degussa) onto mildly heated (ca. 100 °C) substrates through a 1 cm × 1 cm quadrangular mask. Post-treatment of the glass electrodes was performed by sintering them in an oven at 500 °C for 30 min. Plastic electrodes were compacted by room-temperature compressing between stainless steel plates with a manually controlled press (ca. 15 kN/cm$^2$ active area for a few seconds). During compression, the electrode films were covered with a 50 μm PTFE (Teflon®) foil. The resulting film thicknesses were ca. 10 μm for both types of electrodes. After post-treatment the electrode films were sensitized overnight in 0.3 mM solution of the N719 dye (cis-bis(isothiocyanato)bis(2,2′-bipyridyl-4,4′-dicarboxylato)-ruthenium(II) bis-tetrabutyl-ammonium; Solaronix) in absolute ethanol, rinsed and stored in dark, immersed in ethanol.

The cells were assembled on a hot plate using Surlyn film as a sealant and spacer and filled with the electrolyte. Electrical contacts were made of copper tape and conducting silver paint (Electrolube®).

### 2.3. Counter-electrode–counter-electrode cells for EIS measurements

Counter-electrode–counter-electrode cells were prepared similar to the complete solar cells, but the photoelectrode was replaced with a platinized FTO-coated glass and the active area was circular and the diameter either 0.5 or 1 cm. Using two counter-electrodes makes the interpretation of the EIS spectra easier since the effects possibly arising from the photoelectrode are ruled out.

### 2.4. Measurements

*IV* curves for complete solar cells were measured with a custom-built solar simulator equipped with ten 150 W halogen lamps as the radiation source, a temperature-controlled measurement plate and a calibrated monocrystalline silicon reference cell with which the lamps could be adjusted to provide the standard light intensity of 1000 W/m$^2$. The spectral mismatch factor of the simulator, defined with the reference cell and the measured spectral irradiance of the halogen lamps [2,26] was used to make the curves correspond with the standard AM1.5 equivalent illumination.

Impedance spectra were obtained with Zahner Elektrik's IM6 Impedance Measurement Unit controlled with Thales software. Impedance measurements were done in room temperature in the frequency range 100 mHz–100 kHz with 10 mV voltage amplitude at zero DC cell polarization. All cells were measured immediately or maximum a few hours after preparation.

## 3. Results and discussion

### 3.1. Soaking and encapsulation tests

Soaking tests showed drastic differences between the corrosion behavior of the metal samples. The storage protection methods did not improve the corrosion resistance of the

samples, even though chromium is known to be a chemically stable metal and could offer some protection against the electrolyte. This was expected, though, because the layer formed with these methods is actually only a thin, non-uniform film on top of the metal and is not meant to prevent corrosion as such.

In addition to the AAS measurements, the test results were also evaluated visually from the test bottles. Corrosion started to occur on zinc-coated metal samples just in a few days, while the color of the electrolyte changed gradually from deep reddish brown to pale yellow (Fig. 3) as a result of the reduction of the triiodide complex by metallic zinc, based on the following reaction: $Zn + I_3^- \rightarrow Zn^{2+} + 3I^-$.

Triiodide is responsible for the characteristic deep reddish color of the electrolyte, whereas the color of the electrolyte solvent, 3-methoxypropionitrile, varies from pale yellow to colorless, depending on the batch and manufacturer. White zinc iodide precipitate was also observed in some samples after prolonged storage, and in some the reddish color started to return after a few weeks. This was presumably caused by the release of iodine from the zinc iodide when the substance is exposed to light and air [27]. The amount of triiodide in the electrolyte turned out to be the limiting factor for the corrosion reaction, as no further corrosion could be observed after the disappearance of the red color from the electrolyte. The theoretical maximum amount of zinc corroded can be calculated from the known concentrations of the species of the electrolyte and the volume of it in the test bottles. The resulting zinc ion concentration is 3250 mg/l, which agrees quite well with the AAS results presented in Table 2. Reasons for the deviations are probably the concentration variations between different batches of the electrolyte and the uncertainties in measuring the electrolyte for soaking tests. It is also possible that some iodine still exists in the form of $I_2$ in the electrolyte solution and can thus also oxidize the metallic zinc according to the reaction $Zn + I_2 \rightarrow (ZnI_2) \rightarrow Zn^{2+} + 2I^-$. The triiodide complex-forming reaction $I^- + I_2 \rightarrow I_3^-$ is fully shifted towards right in aqueous solutions, but its thermodynamics are significantly dependent on the type of the solvent [28,29]. This means that the formation of triiodide might not be as favored in the electrolyte solvent MePRN as it is in water and some molecular iodine could still be left in the solution. The effects of plain MePRN and TBP on the zinc-coated steels were also separately investigated but neither of these species did cause any damage to the samples.

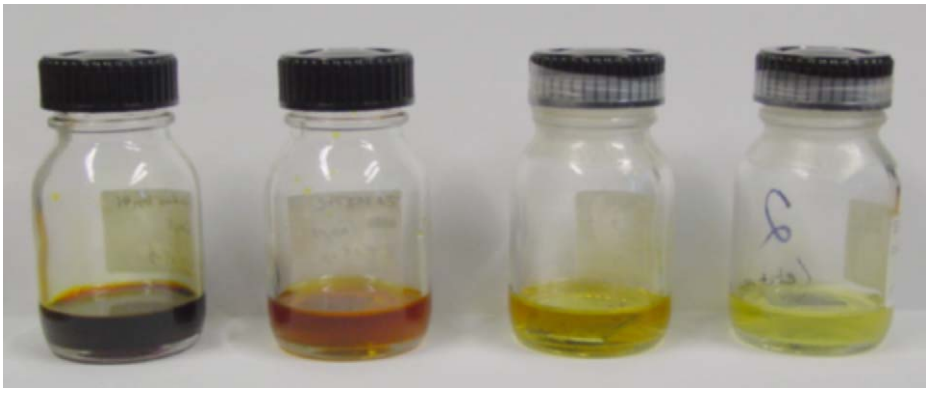

Fig. 3. Electrolyte color change during the soaking tests. Left: initial color; right: final color.

Table 2
Dissolution of the metals into the electrolyte according to the AAS measurements

| Metal | Soaking time before AAS (weeks) | Metal ion concentration (mg/l; average of similar samples) | | | | | |
|---|---|---|---|---|---|---|---|
| | | Zn | Al | Fe[a] | Cr[b] | Ni[b] | Cu |
| Zn-coated carbon steel | 6 | 3711 | – | 0.82 | – | – | – |
| Zn-coated carbon steel, thermally treated | 11 | 2300 | – | 38 | – | – | – |
| Zn–Al-coated carbon steel | 6 | 4154 | 1.5 | – | – | – | – |
| Carbon steel | 11 | – | – | <1 | – | – | – |
| Stainless steel | 6 | – | – | <0.2[c] | <0.2[c] | <0.2[c] | – |
| Copper | 6 | – | – | – | – | – | 982 |

Plain electrolyte was used as the zero standard. Storage protection methods of the metals (i.e. chromation or polymer coating) are not mentioned in the table because the corrosion behaviour of the samples was not affected by them.

[a]Main component (>99%) of carbon steel.

[b]Main components of stainless steel in addition to Fe.

[c]Detection limit of the equipment for the ion in question.

Zinc–aluminum coatings should offer more effective corrosion protection, due to the coating's microstructure created in the alloying. In our soaking tests the corrosion indeed started somewhat slower than with plain zinc-coated samples, but the end result was the same. The main difference between the plain zinc and zinc–aluminum-coated samples was the distribution of the corrosion: plain zinc corroded more locally leaving large areas of the coating intact, whereas in Zn–Al coatings the corrosion was spread evenly with no clearly corroded spots.

Different corrosion rates were also observed for samples stored in different environmental conditions. Corrosion started clearly faster in the samples stored under direct sunlight and the overall corrosion rate, judged from the speed of the electrolyte color change, was fastest for these samples. The return of the reddish color into the electrolyte was also first observed in the sunlight-stored samples supporting the abovementioned.

Thermal treatment improved the zinc coatings' corrosion resistance. After 11 weeks of soaking, the dissolved amount of zinc was 70% of the amount corroded away from the untreated zinc-coated samples and also the electrolyte retained its deep reddish color for several weeks, even if white zinc oxide formation could be visibly noticed only on the edges of the metal plates. Performing the thermal treatment in oxygen-enriched atmosphere instead of normal room air would most probably improve the oxidation process, but the equipment needed for that was not available for this study.

Of the non-coated metals, stainless steel showed no corrosion even after several months of soaking in agreement with the previous studies [17,18]. Also, non-coated carbon steel remained undamaged in the electrolyte for many months, somewhat surprisingly considering the material's poor corrosion stability even against the moisture in the air. The AAS measurements indicated practically no dissolution at all in both cases thus

confirming the visual results. Copper, however, turned out to be very sensitive to the corroding effect of the iodine which is in agreement with previous observations [17].

The most important result of the encapsulation tests was that the corrosion of the protective coating is not detrimental to the cell operation, but the loss of triiodide from the electrolyte, which destroys the whole cell. The electrolyte layer in the cells is very thin, only some tens of micrometers, so that the electrolyte volume and thus the amount of triiodide in contact with the metal surface is too small compared to the amount of reactive metal present for visible corrosion. The reaction rate of corrosion depended also on the coating type as presented in Table 3.

Based on the soaking and encapsulation tests, the materials chosen for further research were stainless and carbon steel. However, it should be observed that carbon steel lacks the corrosion protection required by building legislation which would restrict its use in building integrated DSSC applications.

### 3.2. Charge transfer and series resistances

Table 4 presents the charge transfer ($R_{ct}$) and series resistances ($R_s$) of counter-electrode–counter-electrode cells with different metal electrodes obtained with EIS measurements. Active area of the cells varied between 0.26 and 0.78 $cm^2$ depending on the diameter of the hole in the Surlyn film and the length and width of the electrolyte filling channels. Because platinized FTO-coated glass was used as the other counter-electrode, $R_{ct}$ was first determined from two identical glass counter-electrodes in series platinized in the same batch as the glasses used in the metal counter-electrode cells. Then the contribution

Table 3
Triiodide reduction rates on different metals based on the encapsulation tests

| Metal | Time for complete disappearance of the electrolyte color |
|---|---|
| Zn-coated carbon steel | Max. 1 h |
| Zn-coated carbon steel, thermally treated | Max. 1 day |
| Zn–Al-coated carbon steel | Ca. 3 h |
| Carbon steel | Ca. 2 months[a] |
| Stainless steel | –[b] |
| Copper | Few seconds |

[a]Leakage of air into the encapsulation space via imperfect sealing sped the reaction rate considerably up.
[b]Electrolyte encapsulated on stainless steel is still intact after 12 months of storage.

Table 4
Charge transfer and series resistances for cells with different electrode materials

| Electrode type | $R_{ct}$ ($\Omega\,cm^2$) | $R_s$ ($\Omega$) |
|---|---|---|
| Platinized glass | 13 | 13 |
| Stainless steel | $10^{13}$ | 2 |
| Platinized stainless steel | 19 | 2 |
| Carbon steel | $10^3$ | 2 |
| Platinized carbon steel | 25 | 2 |

of the platinized glass was subtracted from the total $R_{ct}$ obtained with EIS. The numbers in Table 4 represent the averages of similar samples. For non-platinized steels, only the order of magnitude of $R_{ct}$ is shown.

The high values obtained with non-platinized steels indicate poor catalytic activity for the iodide–triiodide redox reaction on the metal surface. When platinized, stainless steel reached a performance level comparable to the standard counter-electrode (platinized FTO-coated glass). The low series resistance of the cells is due to the high conductivity of the metals.

### 3.3. Characterization and performance of the complete solar cells

Based on the EIS results, platinized steels were chosen as the counter-electrode materials for complete DSSC. Figs. 4 and 5 present *IV* curves at 1000 W/m$^2$ AM1.5 equivalent illumination obtained with cells using these counter-electrodes and either glass or plastic as the photoelectrode substrate. Table 5 summarizes the corresponding performance parameters of the cells, i.e., open-circuit voltage ($V_{oc}$), short-circuit current ($I_{sc}$), fill factor (FF) and the energy conversion efficiency ($\eta$). Active areas were 0.32 cm$^2$ for the cells with glass photoelectrodes and 1 cm$^2$ for the cells with plastic photoelectrodes.

The values obtained with platinized metals are comparable to those obtained with the standard cell configuration with all glass substrates. The results for stainless steel are slightly higher or of the same order than those reported in a previous study using a platinizing method for steel similar to this research ($V_{oc}$ 0.576 V, $I_{sc}$ 12.40 mA/cm$^2$, FF 46% and $\eta$ 3.26% [15]). Slight deviations may result from the differences in the electrolyte composition and the manufacturing method of the photoelectrode. Using plastic-deposited photoelectrodes lowers the cell efficiency in all cases because of poorer adhesion between the $TiO_2$ layer and the substrate. This results in lower conductivity on the interface and

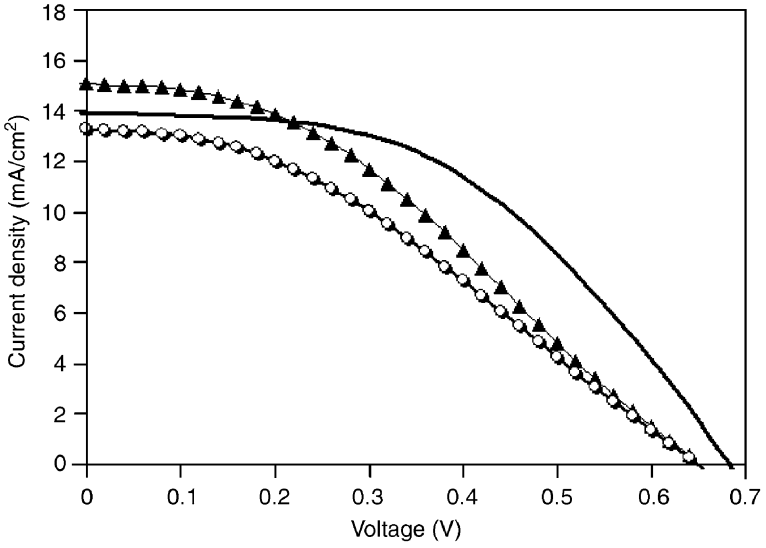


Fig. 4. *IV* curves for solar cells with photoelectrodes on glass substrates, combined with counter-electrodes of platinized stainless steel: (▲) platinized carbon steel, (○) and platinized glass (continuous line).

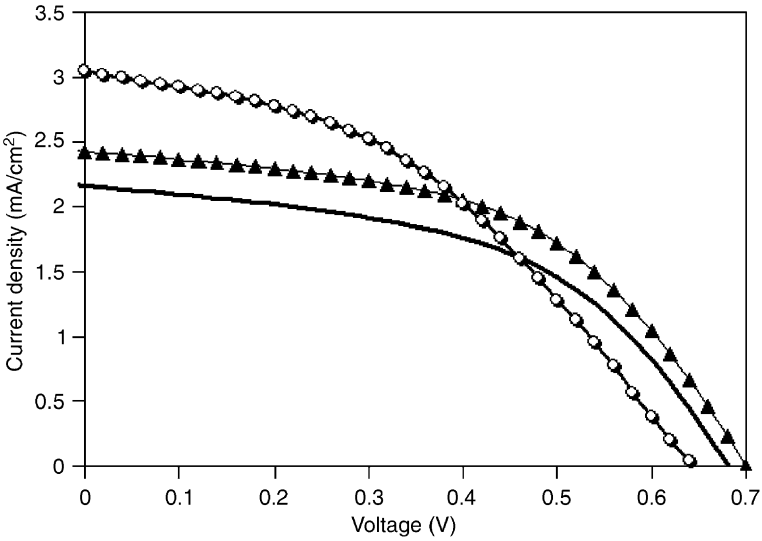


Fig. 5. *IV* curves for solar cells with photoelectrodes on plastic substrates, combined with counter-electrodes of platinized stainless steel: (▲) platinized carbon steel, (○) and platinized glass (continuous line).

Table 5
Performance parameters of the solar cells

| Counter-electrode | Photoelectrode substrate | $V_{oc}$ (V) | $I_{sc}$ (mA/cm$^2$) | FF (%) | $\eta$ (%) |
|---|---|---|---|---|---|
| Platinized stainless steel | Glass | 0.65 | 15.1 | 36 | 3.6 |
| Platinized carbon steel | | 0.65 | 13.3 | 35 | 3.1 |
| Platinized glass | | 0.68 | 13.9 | 48 | 4.6 |
| Platinized stainless steel | Plastic | 0.70 | 2.4 | 51 | 0.9 |
| Platinized carbon steel | | 0.64 | 3.0 | 42 | 0.8 |
| Platinized glass | | 0.69 | 2.2 | 50 | 0.7 |

also the particle interconnections in the electrode film are poorer when compared to the high-temperature sintered glass photoelectrodes. The results in Table 5 with plastic photoelectrode substrates are lower compared to the previous results by our laboratory [21] as full device optimization was not performed here.

The lower FF and efficiencies of the cells with platinized metal counter-electrodes compared to those obtained with platinized FTO glass may be due to the different physico-chemical environment offered by the steel in contrast to the FTO coating. Chemical composition and the crystal structure of the FTO coating differ from those of steel making the energetic structure of the FTO surface possibly more favorable for platinum physi- and/or chemisorption. This is supported by the observation done while assembling the cells: when Surlyn film was melt on top of the platinized steel surface and pulled off, small flakes of platinum coating were clearly attached on the film. For carbon steel, particles of platinum were attached also on a tape when pressed against the platinized surface and pulled off, whereas platinum deposited on FTO glass could not be detached with neither of

the abovementioned methods. Thermal deposition with process parameters for glass is neither the most optimal platinization method for steel [17].

The goodness of the platinum adhesion on the metal is difficult to evaluate from freshly made cells, which supports long-term stability tests for this kind of counter-electrodes. Platinum dissolution rate into the electrolyte is one indication of the adhesion and stability of the catalyst layer [28,30], so determining the order of magnitude of this compared to the standard platinized glass counter-electrodes would give further information about the quality of the steel substrates.

The good thermal conductivity and sturdiness of the metals eased and sped up the cell assembly process, especially the spacer melting step done on a hot plate, yielding durable and compact cells. By optimizing the photoelectrode quality in a DSSC built directly on catalyst-treated steel, at least the same performance as with conducting glass or plastic substrates should be reached due to the better conductivity of the metals. As steel's resistance is negligible compared to that of the FTO glass, it is possible to halve the series resistance of the substrates by replacing the FTO glass with steel, either on the counter- or photoelectrode side.

## 4. Conclusions

In this paper, it has been shown that stainless steel and plain non-coated carbon steel tolerate the corroding effect of the iodine electrolyte used in a DSSC to the extent that these materials could be used as active substrates for this type of solar cells, the substrates acting at the same time as the counter-electrode of the cell. DSSC can be integrated directly on these materials without a protective coating between the metal and the electrolyte layer. A catalyst treatment is necessary since the catalytic activity for the iodide/triiodide redox reaction of the electrolyte is too low for plain steel surfaces. The catalyst can be added for example by thermal platinization of the metals. These catalyzed steel counter-electrodes yield solar cells with good energy conversion efficiencies ($>3\%$, cf. 4–5% obtained with the standard, all-glass substrate cell in this study), sturdy and compact structures and easy and fast manufacturing process. Replacing the expensive conducting glass with metal lowers also the overall price of the cells and improves their long-term stability when more durable materials are used instead of fragile glass. Flexible metal combined with flexible plastic-deposited photoelectrodes is also a promising approach for industrial roll-to-roll manufacturing of the cells.

## Acknowledgements

Financial support from the National Technology Agency of Finland (Tekes) is gratefully acknowledged. The authors thank Ruukki Ltd. and Outokumpu Ltd. for providing the metal sheets, Degussa for $TiO_2$ nanoparticle samples, DuPont for the Surlyn® sheets and Mr. Hannu Revitzer (Helsinki University of Technology) for performing the AAS measurements.

## References

[1] B. O'Regan, M. Grätzel, Nature 353 (1991) 737.
[2] E. Luque, S. Hegedus, Handbook of Photovoltaic Science and Engineering, Wiley, Chichester, 2003.

[3] M. Späth, J. van Roosmalen, P. Sommeling, N. van der Burg, H. Smit, D. Mahieu, N. Bakker, J. Kroon, in: Third World Conference on Photovoltaic Energy Conversion, Osaka, Japan, 2003.
[4] H. Lindström, A. Holmberg, E. Magnusson, S. Lindquist, L. Malmqvist, A. Hagfeldt, Nano Lett. 1 (2001) 97.
[5] H. Lindström, A. Holmberg, E. Magnusson, L. Malmqvist, A. Hagfeldt, J. Photochem. Photobiol. A 145 (2001) 107.
[6] S.A. Haque, E. Palomares, H.M. Upadhyaya, L. Otley, R.J. Potter, A.B. Holmes, J.R. Durrant, Chem. Commun. 24 (2003) 3008.
[7] D. Zhang, T. Yoshida, H. Minoura, Adv. Mater. 15 (2003) 814.
[8] D. Zhang, T. Yoshida, K. Furuta, H. Minoura, J. Photochem. Photobiol. A 164 (2004) 159.
[9] T.N. Murakami, Y. Kijitori, N. Kawashima, T. Miyasaka, Chem. Lett. 32 (2003) 1076.
[10] T.N. Murakami, Y. Kijitori, N. Kawashima, T. Miyasaka, J. Photochem. Photobiol. A 164 (2004) 187.
[11] T. Miyasaka, Y. Kijitori, T.N. Murakami, M. Kimura, S. Uegusa, Chem. Lett. (2002) 1250.
[12] T. Miyasaka, Y. Kijitori, J. Electrochem. Soc. 151 (2004) A1767.
[13] R. Kumar, A.K. Sharma, V.S. Parmar, A.C. Watterson, K.G. Chittibabu, J. Kumar, L.A. Samuelson, Chem. Mater. 16 (2004) 4841.
[14] K.C. Mandal, A. Smirnov, D. Peramunage, R.D. Rauh, Mater. Res. Soc. Symp. Proc. 737 (2003) 739.
[15] S.A. Haque, E. Palomares, H.M. Upadhyaya, L. Otley, R.J. Potter, A.B. Holmes, J.R. Durrant, Chem. Commun. 24 (2003) 3008.
[16] C. Longo, J. Freitas, M. De Paoli, J. Photochem. Photobiol. A: Chem. 159 (2003) 33.
[17] T. Ma, X. Fang, M. Akiyama, K. Inoue, H. Noma, E. Abe, J. Electroanal. Chem. 574 (2004) 77.
[18] X. Fang, T. Ma, M. Akiyama, G. Guan, S. Tsunematsu, E. Abe, Thin Solid Films 472 (2005) 242.
[19] M. Kang, N.-G. Park, K. Ryu, S. Chang, K.-J. Kim, Sol. Energy Mater. Sol. Cells 90 (2006) 574.
[20] T. Meyer, A. Meyer, D. Ginestoux, Proc. SPIE—Int. Soc. Opt. Eng. 4465 (2002) 13.
[21] J. Halme, J. Saarinen, P. Lund, Sol. Energy Mater. Sol. Cells 90 (2006) 887.
[22] J. Halme, M. Toivola, A. Tolvanen, P. Lund, Sol. Energy Mater. Sol. Cells 90 (2006) 872.
[23] J. Van Roosmalen, E. Rijnberg, P. Sommeling, EP 1095387B1, 2004.
[24] N. Vlachopoulos, P. Liska, J. Augustynski, M. Grätzel, J. Am. Chem. Soc. 110 (1988) 1216.
[25] J. Georgieva, S. Armyanov, E. Valova, I. Poulios, S. Sotiropoulos, Electrochim. Acta 51 (2006) 2076.
[26] J. Nelson, The Physics of Solar Cells, Imperial College Press, London, 2003.
[27] http://www.nightingale.org/teachers/fuller/Chemistry%20II/Description%20of%20Chemicals/ZincIodideLab.htm, accessed 27 February 2006.
[28] E. Olsen, G. Hagen, S. Lindquist, Sol. Energy Mater. Sol. Cells 63 (2000) 267.
[29] J. Datta, A. Bhattacharya, K. Kundu, Bull. Chem. Soc. Japan 61 (1988) 1735.
[30] N. Papageorgiou, W. Maier, M. Grätzel, J. Electrochem. Soc. 144 (1997) 876.